RSC Advances

PAPER

View Article Online
View Journal | View Issue

Cite this: *RSC Adv.*, 2020, **10**, 30304

A nanocomposite paper comprising calcium silicate hydrate nanosheets and cellulose nanofibers for high-performance water purification†

Jie Li,[a] Jingshu Zhang,[b] Xuan Wu,[a] Jiajun Zhao,[a] Minjie Wu[a] and Weiwei Huan *[a]

Removal of soluble organic and inorganic contaminants from wastewater to produce clean water has received much attention recently. However, the simultaneous enhancement of water permeability and removal efficiency is still a challenge for filtration membranes. Here, we present a new kind of nanocomposite paper (CSH/CNF) consisting of calcium silicate hydrate (CSH) nanosheets and cellulose nanofibers (CNFs), and demonstrate the rapid water filtration and highly efficient contaminant (*e.g.*, dyes, proteins, and metal ions) adsorption properties. The CNFs can serve as the bridging material to connect the CSH nanosheets to form a porous network structure and vital channels in the CSH/CNF paper for rapid water transportation. The weight ratio of CSH nanosheets in the paper is up to 75–85%. The weight ratio of CSH nanosheets has a significant effect on the water permeability and removal efficiency. The water permeability of the CSH/CNF paper with 82.5 wt% CSH nanosheets reaches as high as 312.7 L m^{-2} h^{-1} bar^{-1}, which is about 14.7 times that of the CSH/CNF paper with 75 wt% CSH nanosheets. Because of the high specific surface area and abundant adsorption sites of CSH nanosheets, the CSH/CNF paper with 82.5 wt% CSH nanosheets exhibits high adsorption capacities and removal efficiencies for methyl blue (242.6 mg g^{-1}, 97.3%), bovine serum albumin (289.2 mg g^{-1}, 98.5%) and Pb^{2+} ions (366.2 mg g^{-1}, 98.2%). The CSH/CNF nanocomposite paper holds great potential for application in environmental wastewater purification.

Received 23rd June 2020
Accepted 10th August 2020

DOI: 10.1039/d0ra05513a

rsc.li/rsc-advances

1. Introduction

Water is an indispensable resource for human survival and the development of nature. With rapid population growth and industrial expansion, public and environmental health are threatened by increasingly serious water pollutants, *e.g.*, heavy metals, dyes, and persistent organic pollutants.[1] Because of waterborne diseases and the shortage of clean water, over 10 000 people die each day including 5000 children under the age of five.[2] Therefore, it is of great importance to develop technologies to remove these contaminants from wastewater. In recent years, various advanced techniques have been adopted for water remediation, including adsorption,[3,4] coagulation,[5,6] oxidation,[7,8] photocatalysis,[9,10] membrane separation,[11,12] and so on. Among them, the membrane separation technologies have attracted much interest owing to their easy manipulation, low energy consumption, time costs, and high separation efficiency.[13] Several nanomaterials were used to prepare porous filtration membranes, such as graphene oxide,[14,15] carbon nanotubes,[16] metal–organic frameworks,[17,18] and cellulose nanofibers.[19,20]

The rapid water transportation and high separation efficiency are two important parameters for practical applications of filtration membranes. However, it is usually difficult to simultaneously realize the two requirements of traditional polymer membranes. The enhancement of pore volume and preparation of ultrathin membranes are two common solutions. The nanofibers-based filtration membranes, *e.g.*, porous electrospun nanofibers,[21–24] have large pore volumes and abundant channels for high water permeability. Even though the electrospun nanofiber membranes have achieved great progresses in water treatment fields, some problems still hinder their applications,[25] such as specific preparation equipment, high voltage, and organic solvents. The graphene-nanomesh/single-walled carbon nanotube membrane[26] polyamide membrane,[27] graphene oxide/polyamide membrane,[28] graphene oxide/oxidized carbon nanotubes/polyethersulfone membrane,[29] and carboxylated cellulose nanocrystal/polyamide/polyethersulfone membrane[30] showed fast separation and high water transportation performances. These nanofiltration membranes need elaborate design and complicated preparation processes. The development of filtration membranes with convenient fabrication process, high separation efficiency and water permeability is highly anticipated.

[a]*Zhejiang Provincial Key Laboratory of Chemical Utilization of Forestry Biomass, Zhejiang A & F University, Lin'an 311300, PR China. E-mail: vivid96@aliyun.com*
[b]*Safety Assessment and Research Center for Drug, Pesticide and Veterinary Drug of Jiangsu Province, Nanjing Medical University, Nanjing 211166, PR China*

† Electronic supplementary information (ESI) available: SEM micrographs, TEM micrographs, nitrogen adsorption–desorption isotherms. See DOI: 10.1039/d0ra05513a

Calcium silicate hydrate (CSH) is a product of the reaction of the Portland cement with water. The abundant hydrated Ca^{2+} ions on the surface can provide active sites to adsorb various chemical entities. Additionally, the CSH has the characteristics of low cost, good stability, and biocompatibility. These features endow excellent adsorption capability to CSH. For example, mesoporous CSH spheres[31] and ultrathin CSH nanosheets[32] with large specific surface areas have exhibited the rapid and high adsorption capacities toward drug, protein, and metal ions. However, the powdered CSH is difficult to separate from aqueous solution after adsorption experiment. The combination of magnetic materials and CSH is a candidate method,[33,34] but the manipulation process is still tedious. In addition, cellulose nanofibers (CNFs) are environmentally friendly materials produced from natural plant fibers.[35] CNFs paper can be facilely prepared by the direct vacuum filtration process. The CNFs paper has been applied for wastewater treatment and purification.[36–38]

In this study, we fabricate a novel kind of CSH/CNF nanocomposite paper with different CSH nanosheets weight ratio and successfully used them as the filter paper for rapid water filtration and highly removal of organic and inorganic contaminants in water purification process. As far as we know, the CSH/CNF nanocomposite filtration paper has not been studied by other researchers and not been used for water purification. The CNFs can serve as the bridging material to connect the CSH nanosheets to form the porous network structure and vital channels of CSH/CNF paper. The CSH nanosheets with high specific surface area provide abundant active sites for highly efficient adsorption property. The effect of the CSH nanosheets weight ratio in the nanocomposite paper on the porous structure, porosity, pore size distribution, water permeability, and filtering adsorption capacities toward dye, protein, and metal ion are investigated. Benefiting from the unique properties of CSH nanosheets and CNFs, the CSH/CNF paper can simultaneously achieve enhancement of water permeability and removal efficiency during the filtration process. The CSH/CNF paper provides a promising opportunity for highly efficient removal of pollutants in practical water treatment and purification applications.

2. Experimental

2.1 Materials and reagents

Calcium chloride ($CaCl_2$), sodium silicate nonahydrate ($Na_2SiO_3 \cdot 9H_2O$), lead chloride ($PbCl_2$), and chromium chloride hexahydrate ($CrCl_2 \cdot 6H_2O$) were obtained from Sinopharm Chemical Reagent Co., Ltd. Methyl blue, congo red, and bovine serum albumin were received from Aladdin Industrial Corporation. 2,2,6,6-tetramethylpiperidine-1-oxyl free radical (TEMPO)-oxidized cellulose nanofibers (CNFs) were purchased from Tianjin Woodelfbio Cellulose Co., Ltd. All the obtained chemicals were received without further purification.

2.2 Synthesis of calcium silicate hydrate (CSH) nanosheets

In detail, 852 mg of $Na_2SiO_3 \cdot 9H_2O$ was dissolved in 50 mL of deionized water to obtain solution A, 708 mg of $CaCl_2$ was dissolved in 5 mL of deionized water to obtain solution B. The solution B was slowly injected into solution A with a constant rate of 2.5 mL h^{-1} under magnetic stirring at room temperature. When the solution was completely added, the suspension solution was stirred for another 4 h. The product was filtered, washed sequentially with deionized water and ethanol for three times, and dried at 60 °C overnight in an oven.

2.3 Preparation of calcium silicate hydrate/cellulose nanofibers (CSH/CNF) paper

The CSH/CNF nanocomposite paper was prepared through a vacuum filtration approach. Typically, a certain amount of CSH nanosheets and CNFs was dispersed in 50 mL of deionized water under magnetic stirring. The suspension was poured onto a filter membrane and filtered under vacuum. After washing with ethanol for three times and drying at 75 °C for 30 min, the CSH/CNF nanocomposite paper was obtained. The total amount of CSH nanosheets and CNFs was 50 mg. Five samples with different CSH weight ratio of 85 wt%, 82.5 wt%, 80 wt%, 77.5 wt% and 75 wt% were prepared.

2.4 Material characterization

Scanning electron microscopy (SEM) micrograph and elemental mapping analysis were obtained using a field-emission scanning electron microscope (Hitachi S-4800). Transmission electron microscopy (TEM) micrograph was recorded with a transmission electron microscope (JEOL F2100). The porosity was measured by the mercury intrusion method (AutoPore IV 9510, Micromeritics). Thermogravimetric analysis (TGA) was carried out using a thermal analyzer (STA 409/PC, Netzsch) in flowing air at a heating rate of 10 °C min^{-1}. The Brunauer–Emmett–Teller (BET) specific surface area was measured using a surface area analyzer (Tristar II 3020, Micromeritics). Fourier transform infrared (FTIR) spectroscopy was recorded with a FTIR spectrometer (Thermo Nicolet Nexus 470). X-ray powder diffraction (XRD) pattern was recorded using an X-ray diffractometer (Rigaku D/max 2550 V, Cu Kα radiation, $\lambda = 1.54178$ Å). The pore size distribution curve was analysed using a pore size analyzer (3H-2000, Beshide Instrument Technology) based on a bubble point method. The zeta potential was measured by a potential analyzer (ZetaPlus, Brookhaven, USA).

2.5 Adsorption capacity of CSH/CNF paper

The adsorption experiment was executed in a static mode. The CSH/CNF paper (10 mg) was cut into small pieces with sizes of about 5 × 5 mm and separately placed in the aqueous solution containing dye, protein, or metal salt with a volume of 5 mL and the concentration of 2.0 mg mL^{-1}. After the filtering adsorption of CSH/CNF paper, the residual concentration was carefully measured. The concentrations of dye and protein were determined by UV-visible absorption spectroscopy (Shimadzu UV-1700). The concentration of metal ion was analysed by an inductively coupled plasma-optical emission spectrometer (ICP-OES, PerkinElmer, Optima 5300DV).

2.6 Continuous filtering removal performance of CSH/CNF paper

The continuous filtration experiment was implemented with a vacuum filter. The CSH/CNF paper was fixed on a sand core funnel with an inner diameter of 20 mm. 30 mL of pure water or aqueous solution containing dye, protein or metal salt with a concentration of 10 mg L^{-1} was filtering through the CSH/CNF paper under the pressure of 1 bar. The water permeability was calculated by permeability $= V/(Atp)$, where V, A, t, and p is the filtered aqueous volume (L), the filtering area (m^2), filtering time (h), and suction pressure (bar), respectively. The removal percentage was calculated by percentage $= (M_0 - M_1)/M_0 \times 100\%$, where M_0 and M_1 are the concentration of dye, protein, and metal ion in the original solution and filtrate (mg L^{-1}).

3. Results and discussion

3.1 Characterization of CSH/CNF nanocomposite paper

The CSH/CNF nanocomposite paper was fabricated by the self-assembly approach of CSH nanosheets and CNFs in the vacuum filtration process, as shown in Fig. 1a. The uniformly dispersed CSH nanosheets aqueous suspension was mixed with uniformly dispersed CNFs aqueous suspension. After suction filtration, the CSH nanosheets and CNFs self-assembled into a free-standing nanocomposite paper with white color. The CNFs play extremely important roles in forming the paper structure. The CNFs serve as the bridging material to connect the CSH nanosheets through van der Waals force and coordination interactions, which can form the continuous porous network structure of CSH/CNF paper (Fig. 1b). The CSH/CNF paper has flexible property, it can be bent using a tweezer. As a comparison, some independent particles are obtained when the CSH nanosheets were only employed as the building material in the same vacuum filtration process (Fig. 1c).

SEM and TEM micrographs of CSH nanosheets are shown in Fig. 2a, b and S1 (ESI).† The CSH sample comprises a hierarchical morphology formed by the self-assembly of the crumpled nanosheets, which shows the porous structure. The CSH nanosheets composite has size of hundreds of nanometers. In the absence of CNFs, the CSH nanosheets cannot form a free-standing paper structure (Fig. 1c). The CNFs have diameters range from about 10 to 200 nm (Fig. S2, ESI†). Five kinds of CSH/CNF papers with different CSH weight ratios (85, 82.5, 80, 77.5, and 75 wt%) were prepared, and the corresponding SEM micrographs are shown in Fig. 2c–l. The CSH/CNF papers have abundant pores on the surfaces. It is noteworthy that the surface porous size of CSH/CNF paper with 85 and 82.5 wt% CSH nanosheets are larger than that of CSH/CNF paper with 80, 77.5 and 75 wt% CSH. The CNFs can serve as the bridging material to link and interweave the CSH nanosheets, and the nanocomposite further forms the porous network structure of CSH/CNF paper. With increasing the weight ratio of CNFs, the porous structure of CSH/CNF paper is filled by CNFs, and the porous size is decreased. The porosities are measured to 79.0, 78.1, 77.1, 74.8, and 71.9% for CSH/CNF paper with 85, 82.5, 80, 77.5 and 75 wt% CSH, respectively. The result is consist with the SEM characterization results.

The EDS element mappings exhibit the distribution of Ca, Si, O, and C elements in the CSH/CNF paper with 82.5 wt% CSH. As shown in Fig. 3, the CSH nanosheets and CNFs are uniformly dispersed in the CSH/CNF paper. The CNFs as bridging material connect the CSH nanosheets with surrounding ones to form the macroscopic structure of CSH/CNF paper.

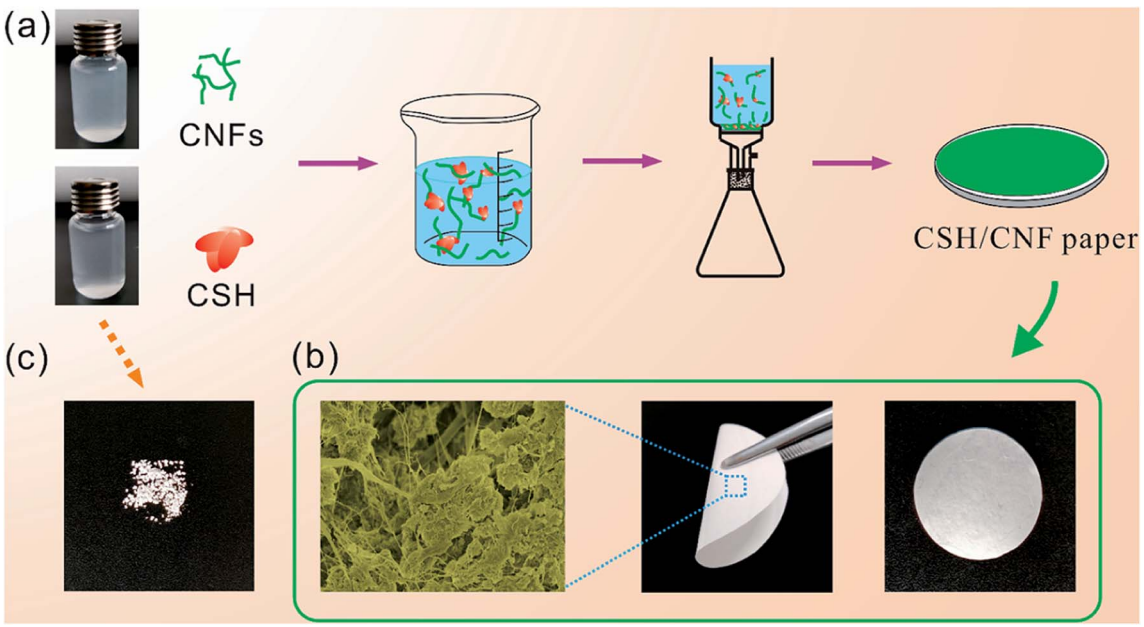

Fig. 1 (a) Schematic illustration of the CSH nanosheets and CNFs as building blocks for the preparation of CSH/CNF nanocomposite paper; (b) the digital images and microstructure of CSH/CNF paper with 82.5 wt% CSH; (c) the digital image of CSH powder using CSH nanosheets as building block by the same vacuum filtration process.

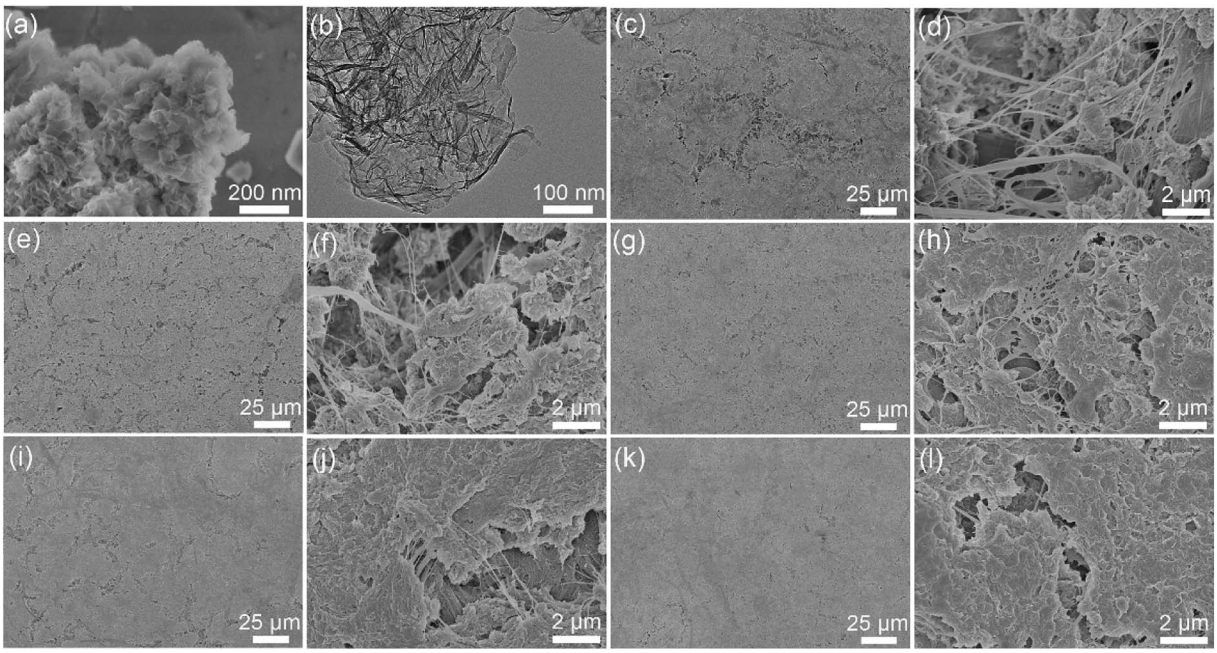

Fig. 2 (a and b) SEM and TEM micrographs of CSH nanosheets; (c–l) SEM micrographs of CSH/CNF paper with different CSH nanosheets weight ratios: (c and d) 85 wt%; (e and f) 82.5 wt%; (g and h) 80 wt%; (i and j) 77.5 wt%; and (k and l) 75 wt%.

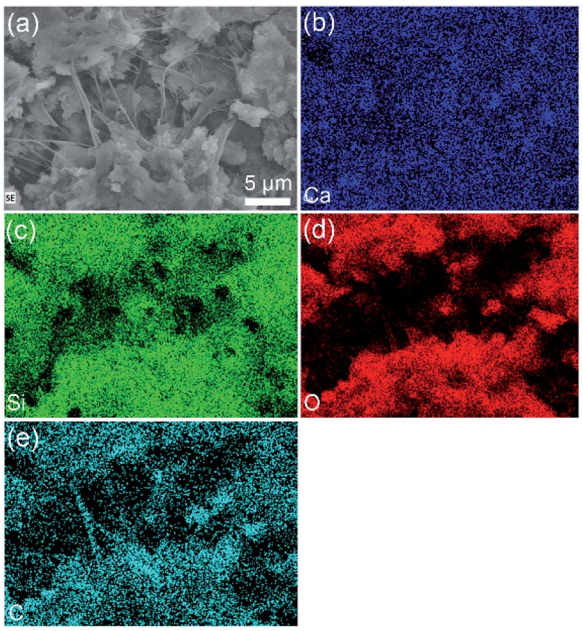

Fig. 3 (a) SEM micrograph of CSH/CNF paper with 82.5 wt% CSH; (b–e) the corresponding EDS elemental mappings of CSH/CNF paper with 82.5 wt% CSH.

The thermogravimetric analysis (TGA) curves of CSH nanosheets, CNFs, and CSH/CNF paper with different CSH weight ratio are shown in Fig. 4a. The total weight loss of CSH nanosheets is about 24.0% at temperatures range from 26 to 910 °C, which can be assigned to the adsorbed water and crystal water. The CNFs are completely decomposed at about 450 °C. With decreasing the weight ratios of CSH, the residual weights of CSH/CNF paper are decreased. The weight losses of CSH/CNF paper can be attributed to the organic component of CNFs, adsorbed water and crystal water. The TGA analysis result is consistent with the preparation parameters of CSH/CNF paper.

The CSH nanosheets, CNFs, and CSH/CNF paper with different CSH weight ratio were characterized by the Brunauer–Emmett–Teller (BET) surface area analyzer. As shown in Fig. S3 (ESI),† the BET specific surface area of the CSH nanosheets is 420.26 $m^2 g^{-1}$. The high BET specific surface area of CSH is due to the hierarchical structure formed from the nanosheets. The BET specific surface area of CNFs is only 4.69 $m^2 g^{-1}$ (Fig. S4, ESI†). The BET specific surface area of CSH/CNF paper decreases from 62.11 $m^2 g^{-1}$ for 85 wt% CSH to 47.19 $m^2 g^{-1}$ for 75 wt% CSH (Fig. 4b), showing the same trend as the porosity of CSH/CNF paper.

Fourier transform infrared (FTIR) spectra are recorded to study the chemical composition. As shown in Fig. 4c, The FTIR spectrum of CSH nanosheets has a characteristic absorption peak at 970 cm^{-1}, which is ascribed to the Si–O vibration. The FTIR spectrum of CNFs has the absorption peaks at 2918 and 669 cm^{-1}, they can be assigned to C–H stretching and –OH out-of-plane bending, respectively. The absorption peaks at 3423 and 1637 cm^{-1} can be ascribed to the adsorbed water. In the FTIR spectrum of CSH/CNF with 82.5 wt% CSH, the characteristic absorption peaks of CSH nanosheets and CNFs can be found simultaneously.

Fig. 4d shows the XRD patterns of CSH nanosheets, CNFs and CSH/CNF paper with 82.5 wt% CSH. The diffraction peaks of CSH nanosheets are consistent with calcium silicate ($Ca_5Si_6O_{16}(OH)_2 \cdot 8H_2O$, JCPDS no. 29-0331). The diffraction peaks at $2\theta = 14.8°$ and 22.7° correspond to the (101) and (002) crystal

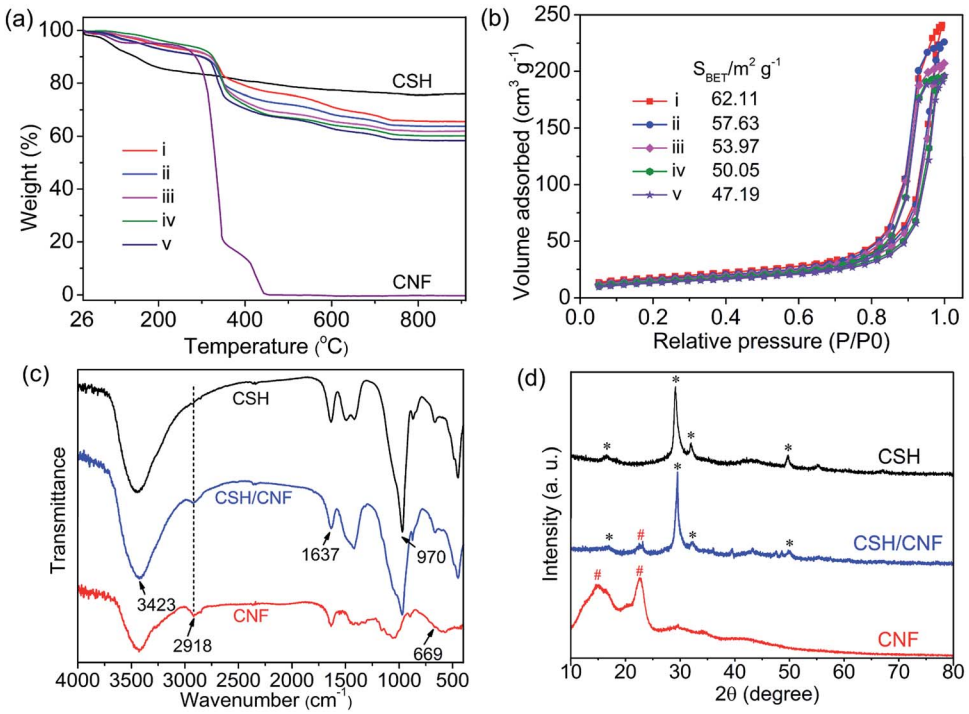

Fig. 4 (a) TGA curves of CSH nanosheets, CNFs, and CSH/CNF paper with different CSH weight ratios: (i) 85 wt%; (ii) 82.5 wt%; (iii) 80 wt%; (iv) 77.5 wt%; and (v) 75 wt%. (b) Nitrogen adsorption–desorption isotherms of CSH/CNF paper with different CSH weight ratios: (i) 85 wt%; (ii) 82.5 wt%; (iii) 80 wt%; (iv) 77.5 wt%; and (v) 75 wt%. (c) FTIR spectra and (d) XRD patterns of CSH nanosheets, CNFs, and CSH/CNF paper with 82.5 wt% CSH.

planes of CNFs. The CSH/CNF paper has the mixed phases of CSH nanosheets and CNFs.

The pore size distribution of CSH/CNF paper was measured by the bubble point method.[39,40] As shown in Fig. 5, the average pore diameters of the CSH/CNF paper are 689.3, 487.5, 369.8, 265.0 and 219.8 nm for the CSH weight ratios ranging from 85 to 75%, respectively. By the increased addition of CSH nanosheets, the pore size of the nanocomposite paper can be significantly enhanced. Obviously, the average pore size of the CSH/CNF paper can be regulated by the CSH weight ratio. The

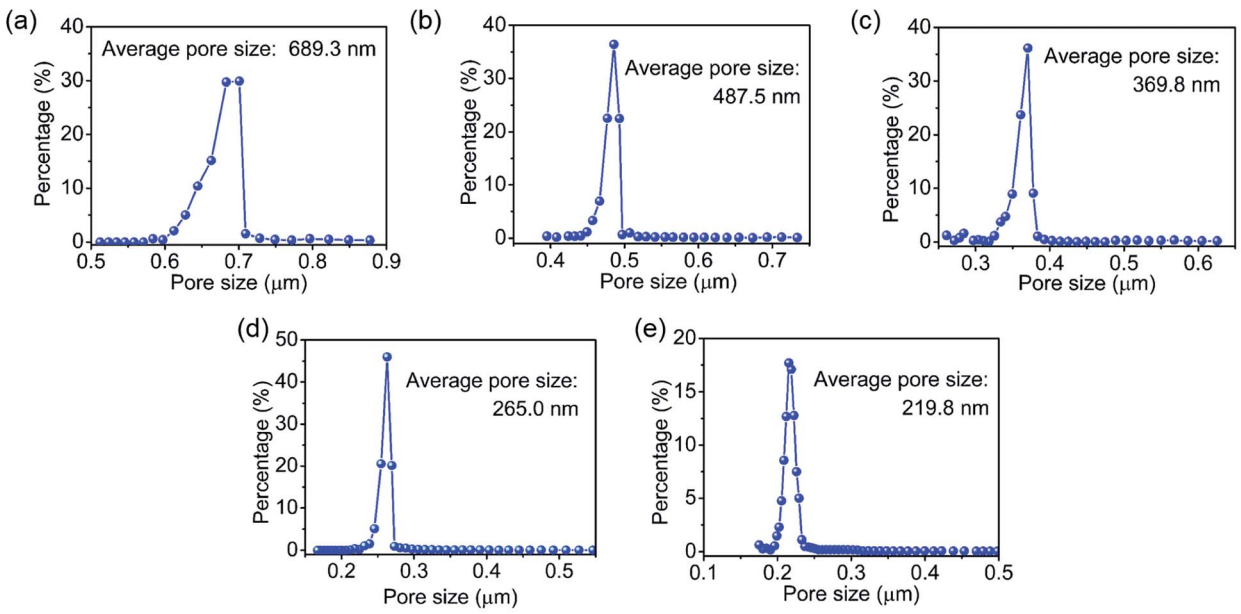

Fig. 5 Pore size distribution curves of the CSH/CNF paper with different CSH weight ratios: (a) 85 wt%; (b) 82.5 wt%; (c) 80 wt%; (d) 77.5 wt%; and (e) 75 wt%.

zeta potential of CNFs is determined to −24.76 mV, CNFs have a large number of COO^- groups. The CSH nanosheets have abundant hydrated Ca^{2+} ions on the surface, Ca^{2+} ions and COO^- groups can form the strong coordination interactions. The CSH nanosheets intertwine with CNFs by the van der Waals force and coordination interactions. The nanocomposite is self-assembled into the porous network structure. As the weight ratio of CSH nanosheets enhances, the interactions between the CNFs and CSH is decreased, leading to an increase in the average pore size of CSH/CNF paper.

3.2 Filtering adsorption performance of CSH/CNF paper

The pure water permeability of the CSH/CNF paper with different CSH weight ratio was firstly investigated. As shown in Fig. 6a, with increasing the CSH weight ratio, the water permeabilities of CSH/CNF paper are significantly increased. For example, the CSH/CNF paper with 82.5 wt% CSH can reach 312.7 L m^{-2} h^{-1} bar^{-1}, which is 14.7 times that of CSH/CNF paper with 75 wt% CSH (21.3 L m^{-2} h^{-1} bar^{-1}). The water permeability of CSH/CNF paper with 82.5 wt% CSH is significantly higher than that of nanofiltration membranes.[26–30] Further detailed comparison is presented in Section 3.3. The low water flux of CSH/CNF paper with relatively low CSH weight ratio may due to the low porosity and dense structure.

The CSH/CNF paper was further employed for the purification of wastewater containing organic and inorganic contaminants (*e.g.*, dye, protein, and metal ion) through pressure-driven continuous filtering adsorption process. As shown in Fig. 6b, the CSH/CNF paper was fixed on a sand core funnel filter. The dye solutions, *e.g.*, methyl blue and congo red are filtered across the CSH/CNF paper. Fig. 6c shows the digital images of congo red and methyl blue aqueous solutions before and after filtering adsorption using the CSH/CNF paper with 82.5 wt% CSH. It is visibly observed that the dye solutions are discolored after filtration. The negatively charged dye molecules are effectively adsorbed by the abundant hydrated Ca^{2+} ions on CSH/CNF paper.

The effect of CSH weight ratio of the CSH/CNF paper on the filtration performance was investigated. As shown in Fig. 6d, the water permeability of methyl blue aqueous solution for CSH/CNF paper with different CSH weight ratio is similar to that of pure water. The removal efficiency of methyl blue for CSH/CNF paper with 75 wt% CSH is as high as 99.6%, but the water permeability is as low as 22.6 L m^{-2} h^{-1} bar^{-1}. With further increasing the CSH weight ratio to 82.5 wt%, the water permeability of methyl blue aqueous solution is significantly enhanced to 308.6 L m^{-2} h^{-1} bar^{-1} with the removal efficiency of 97.3%. Owing to the porous structure, high specific surface area, and abundant adsorption sites on the CSH nanosheets, the CSH/CNF paper with 82.5 wt% CSH can simultaneously achieve the high water permeability and removal efficiency.

When the addition weight ratio of CSH further rises, the water permeability of CSH/CNF paper with 85 wt% CSH markedly increases to 439.6 L m^{-2} h^{-1} bar^{-1}, but the removal efficiency decreases to 86.9%. The previous characterization results show that the CSH/CNF paper with 85 wt% has the highest porosity and average pore size among these five kinds of CSH/CNF papers. The CSH/CNF paper with 85 wt% CSH can obtain the highest water permeability, but the fast flow decreases the changes for adequate adsorption of methyl blue molecules.

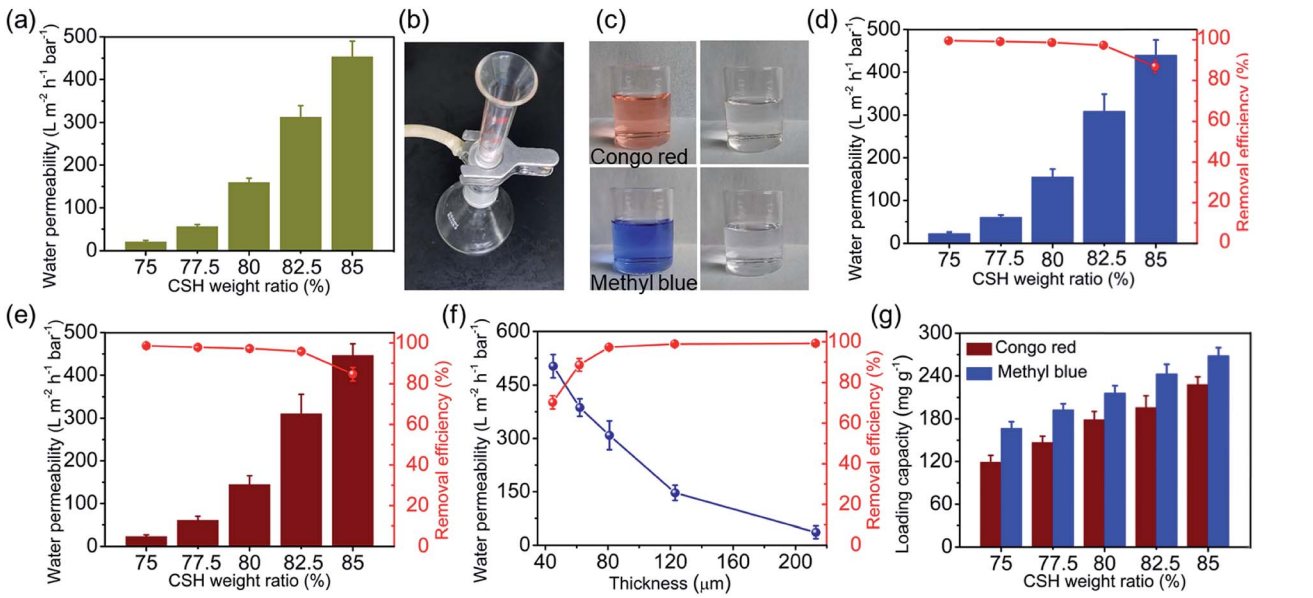

Fig. 6 (a) Pure water permeability of the CSH/CNF paper with different CSH weight ratio; (b) the digital image of the pressure-driven continuous filter using the CSH/CNF paper; (c) the digital images of congo red and methyl blue aqueous solutions before and after passing the CSH/CNF paper with 82.5 wt% CSH; (d) water permeability and removal efficiency of methyl blue aqueous solution for CSH/CNF paper with different CSH weight ratio; (e) water permeability and removal efficiency of congo red aqueous solution for CSH/CNF paper with different CSH weight ratio; (f) water permeability and removal efficiency of methyl blue *vs.* the thickness of CSH/CNF paper with 82.5 wt% CSH; (g) adsorption capacity of CSH/CNF paper with different CSH weight ratio for congo red and methyl blue.

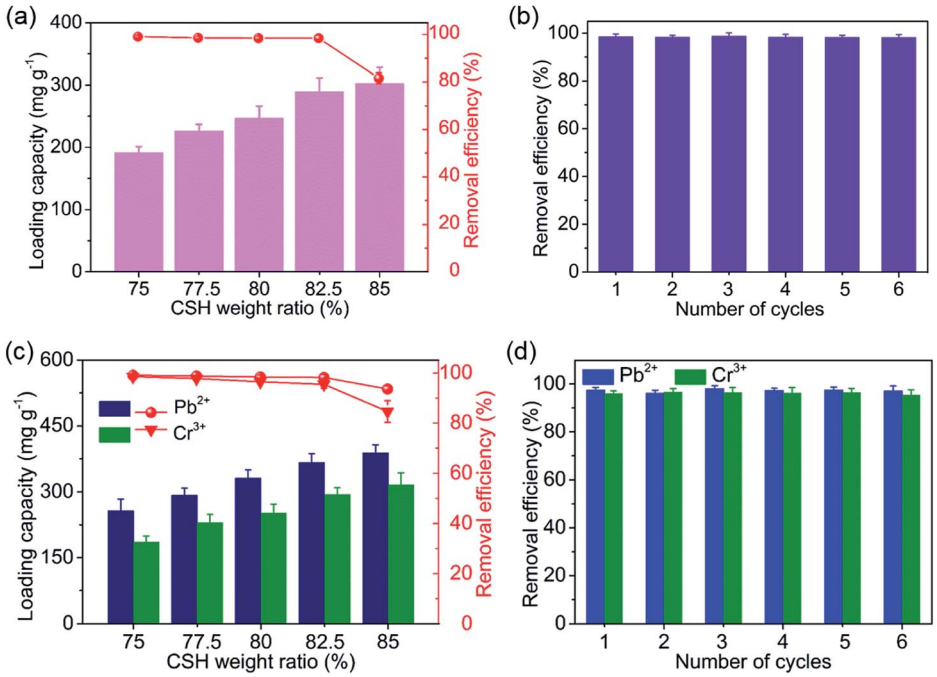

Fig. 7 (a) Loading capacity and removal efficiency of CSH/CNF paper with different CSH weight ratios towards bovine serum albumin; (b) removal efficiency change of bovine serum albumin during recycling tests; (c) loading capacity and removal efficiency of CSH/CNF paper with different CSH weight ratio towards Pb^{2+} and Cr^{3+} ions; (d) removal efficiency change of Pb^{2+} and Cr^{3+} ions during recycling tests.

Another kind of dye was adopted to determine the filtering adsorption ability. As shown in Fig. 6e, the filtering adsorption performance of the CSH/CNF paper with 82.5% CSH for congo red is similar to that of methyl blue. The water permeability and removal efficiency of CSH/CNF paper with 82.5 wt% CSH for congo red is 310.8 L m^{-2} h^{-1} bar^{-1} and 95.8%, respectively.

The thickness of CSH/CNF paper has a significantly impact on the water permeability and removal efficiency of methyl blue. Methyl blue aqueous solution was filtered through the CSH/CNF paper (82.5 wt% of CSH) with different thickness ranges from 45 to 213 μm. The enhancement of the thickness of CSH/CNF paper leads to an obvious declination of water permeability (Fig. 6f). The water permeability of CSH/CNF paper with thickness of 45 μm is 13.8 times that of CSH/CNF paper with thickness of 213 μm. While the removal efficiency of methyl blue exhibits a positive enhancement with the increase of paper thickness. The removal efficiency can reach above 97.0% when the thickness of CSH/CNF paper is below about 80 μm.

The adsorption capacity of CSH/CNF paper with different CSH weight ratio was investigated. As shown in Fig. 6g, with enhancing the CSH weight ratio, the adsorption capacities of CSH/CNF paper with 82.5 wt% CSH are linearly increased for both methyl blue and congo red. This phenomenon is consist with the BET specific surface area analyse result. The adsorption capacity of CSH/CNF paper with 82.5 wt% CSH is 242.6 mg g^{-1} and 195.9 mg g^{-1} for methyl blue and congo red, respectively. The abundant hydrated Ca^{2+} ions on CSH nanosheets contribute to the high adsorption capacity of CSH/CNF paper.

Moreover, the bovine serum albumin was further chosen for determining the adsorption and filtration removal performance of CSH/CNF paper. As shown in Fig. 7a, with increasing the CSH weight ratio, the adsorption capacity of CSH/CNF paper towards bovine serum albumin is linearly enhanced. The adsorption capacity of CSH/CNF paper with 82.5 wt% CSH is 289.2 mg g^{-1}. The bovine serum albumin biomolecules are adsorbed on the CSH nanosheets in CSH/CNF paper through the electrostatic interactions between COO^- groups in bovine serum albumin and hydrated Ca^{2+} ions in CSH nanosheets. When the bovine serum albumin aqueous solution is filtering through the CSH/CNF paper with different CSH weight ratio, the removal efficiency is slowly declined, but further significantly declined. For example, the removal efficiency of CSH/CNF paper with 75 and 82.5 wt% CSH is 99.1% and 98.5%, but the removal efficiency of CSH/CNF paper with 85 wt% CSH is reduced to 81.6%. This result may impute to the inadequate adsorption during fast water flow process. In addition, the filtering adsorption test is continuously repeated for six cycles, no obvious decrease in the removal efficiency is observed (Fig. 7b). The removal efficiency of bovine serum albumin can be retained above 98.1%, revealing the good recyclability of CSH/CNF paper.

Heavy metal ions are the common pollutants in wastewater. The adsorption and filtering performance of CSH/CNF paper towards heavy metal ions is investigated. As shown in Fig. 7c, the adsorption capacity of CSH/CNF for Pb^{2+} and Cr^{3+} ions is increased with enhancing the CSH weight ratio. This result is due to the enhanced specific surface area and adsorption sites of hydrated Ca^{2+} ions of CSH nanosheets. Pb^{2+} and Cr^{3+} ions are adsorbed on the CSH nanosheets in CSH/CNF paper through ion exchange processes. The removal efficiencies of CSH/CNF paper with CSH weight ratio below 82.5 wt% are slightly different, but the CSH/CNF paper with 85 wt% CSH has the lowest removal efficiencies. Overall, the CSH/CNF paper with 82.5 wt% CSH has

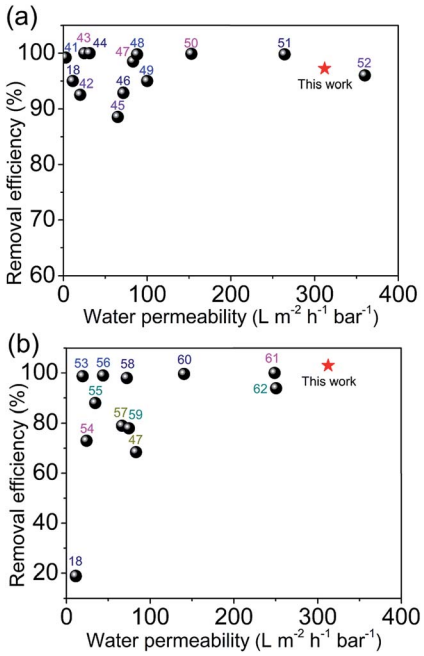

Fig. 8 (a) Comparison of the water permeability and MB removal efficiency of the CSH/CNF paper with 82.5 wt% CSH in this work with some filtration membranes reported in the literature; (b) comparison of the water permeability and Pb^{2+} ion removal efficiency of the CSH/CNF paper with 82.5 wt% CSH in this work with some filtration membranes reported in the literature.

the optimal adsorption capacities (366.2 and 294.2 mg g^{-1}) and removal efficiencies (98.2 and 95.5%) for Pb^{2+} and Cr^{3+} ions. The recyclability is studied by continuously filtering process for six cycles, as shown in Fig. 7d, the removal efficiencies for Pb^{2+} and Cr^{3+} ions have no obvious declines. Therefore, the CSH/CNF paper with high adsorption capacity and adsorption efficiency is a promising material for high-efficiency removal of organic and inorganic pollutants in wastewater.

3.3 Comparison of water permeability and removal efficiency for MB and Pb^{2+} ion with some filtration membranes reported in the literature

Fig. 8 shows the comparison of the water permeability and removal efficiencies of MB and Pb^{2+} ion of the CSH/CNF paper with 82.5 wt% CSH with some filtration membranes reported in the literature. In Fig. 8a, although the removal efficiencies of MB of some filtration membranes were above 85%,[18,41–52] most of the water permeability was below 300 L m^{-2} h^{-1} bar^{-1}. The adsorption performance of CSH/CNF paper with 82.5 wt% CSH for MB is comparable to or higher than these filtration membranes. In addition, even though some reported filtration membranes enable efficient adsorption of Pb^{2+} ion (Fig. 8b), their water permeabilities were generally lower than 260 L m^{-2} h^{-1} bar^{-1}.[18,47,53–62] The adsorption ability of CSH/CNF paper with 82.5 wt% CSH for Pb^{2+} ion is higher than these filtration membranes. The CSH/CNF paper can simultaneously achieve the high water permeability and removal efficiency for dye molecules and metal ions in the filtration process.

4. Conclusions

In this study, a new kind of nanocomposite paper for rapid water filtration and highly efficient contaminant removal efficiency is developed using calcium silicate hydrate nanosheets and cellulose nanofibers as building blocks. The CNFs can serve as the bridging material to connect the CSH nanosheets to form the porous network structure and vital channels of CSH/CNF paper. By adjusting the addition weight ratio of CSH nanosheets, the porous structure, porosity, pore size distribution, and specific surface area can be controlled. The optimized pure water permeability of the CSH/CNF paper with 82.5 wt% CSH is as high as 312.7 L m^{-2} h^{-1} bar^{-1}, which is about 14.7 times that of the CSH/CNF paper with 75 wt% CSH. More importantly, the CSH/CNF paper with 82.5 wt% CSH has high adsorption capacities and removal efficiencies for dye, protein, and metal ion, *e.g.*, methyl blue (242.6 mg g^{-1}, 97.3%), bovine serum albumin (289.2 mg g^{-1}, 98.5%) and Pb^{2+} ion (366.2 mg g^{-1}, 98.2%). Therefore, the addition of CSH nanosheets is an effective method for improving both the water flux and filtering adsorption efficiency. The CSH/CNF paper has promising applications for highly efficiency environmental wastewater purification in water sustainability fields.

Conflicts of interest

There are no conflicts to declare.

Acknowledgements

The authors gratefully acknowledge the financial support from the Zhejiang Public Welfare Technology Research/Rural Agriculture (No. LGN18B010001), and the Open Project of the Laboratory of Modern Toxicology of Ministry of Education, Nanjing Medical University (No. NMUAMT201807).

References

1 P. J. J. Alvarez, C. K. Chan, M. Elimelech, N. J. Halas and D. Villagan, *Nat. Nanotechnol.*, 2018, **13**, 634–641.
2 R. M. Pink, *Water Rights in Southeast Asia and India*, Palgrave Macmillan, New York 2016.
3 M. Sarcletti, D. Vivod, T. Luchs, T. Rejek, L. Portilla, L. Mueller, H. Dietrich, A. Hirsch, D. Zahn and M. Halik, *Adv. Funct. Mater.*, 2019, **29**, 1805742.
4 A. Misra, C. Zambrzycki, G. Kloker, A. Kotyrba, M. H. Anjass, I. F. Castillo, S. G. Mitchell, R. Guettel and C. Streb, *Angew. Chem., Int. Ed.*, 2020, **59**, 1601–1605.
5 B. Shi, G. Li, D. Wang, C. Feng and H. Tang, *J. Hazard. Mater.*, 2007, **143**, 567–574.
6 H. M. Cui, X. Huang, Z. C. Yu, P. Chen and X. L. Cao, *RSC Adv.*, 2020, **10**, 20231–20244.
7 X. H. Dai, H. X. Fan, C. Y. Yi, B. Dong and S. J. Yuan, *J. Mater. Chem. A*, 2019, **7**, 6849–6858.
8 J. Ren, H. Li, N. Li, Y. Song, J. Chen and L. Zhao, *RSC Adv.*, 2020, **10**, 17163–17170.

9 Y. Li, Y. Jiang, Z. Ruan, K. Lin, Z. Yu, Z. Zheng, X. Xu and Y. Yuan, *J. Mater. Chem. A*, 2017, **5**, 21300–21312.
10 E. Kusiak-Nejman and A. W. Morawski, *Appl. Catal., B*, 2019, **253**, 179–186.
11 Y. Liu, D. Shen, G. Chen, A. A. Elzatahry, M. Pal, H. Zhu, L. Wu and J. Lin, *Adv. Mater.*, 2017, **29**, 1702274.
12 Q. Zhang, S. Bolisetty, Y. Cao, S. Handschin, J. Adamcik, Q. Peng and R. Mezzenga, *Angew. Chem., Int. Ed.*, 2019, **58**, 6012–6016.
13 L. Yu, S. Ruan, X. Xu, R. Zou and J. Hu, *Nano Today*, 2017, **17**, 79–95.
14 F. Fei, L. Cseri, G. Szekely and C. F. Blanford, *ACS Appl. Mater. Interfaces*, 2018, **10**, 16140–16147.
15 L. Chen, Y. Li, L. Chen, N. Li, C. Dong, Q. Chen, B. Liu, Q. Ai, P. Si, J. Feng, L. Zhang, J. Suhr, J. Lou and L. Ci, *Chem. Eng. J.*, 2018, **345**, 536–544.
16 Y. Dong, L. Ma, C. Y. Tang, F. Yang, X. Quan, D. Jassby, M. J. Zaworotko and M. D. Guiver, *Nano Lett.*, 2018, **18**, 5514–5521.
17 J. E. Efome, D. Rana, T. Matsuura and C. Q. Lan, *J. Mater. Chem. A*, 2018, **6**, 4550–4555.
18 L. Zhu, L. Zong, X. Wu, M. Li, H. Wang, J. You and C. Li, *ACS Nano*, 2018, **12**, 4462–4468.
19 M. A. Lucchini, E. Lizundia, S. Moser, M. Niederberger and G. Nystrom, *ACS Appl. Mater. Interfaces*, 2018, **10**, 29599–29607.
20 C. Zhu, P. Liu and A. P. Mathew, *ACS Appl. Mater. Interfaces*, 2017, **9**, 21048–21058.
21 Q. Liu, Z. W. Chen, X. Y. Pei, C. S. Guo, K. Y. Teng, Y. L. Hu, Z. W. Xu and X. M. Qian, *J. Mater. Sci.*, 2020, **55**, 893–924.
22 Y. Wang, B. Wang, Q. Wang, J. Di, S. Miao and J. Yu, *ACS Appl. Mater. Interfaces*, 2019, **11**, 1672–1679.
23 Y. Xu, D. Yuan, J. Bao, Y. Xie, M. He, Z. Shi, S. Chen, C. He, W. Zhao and C. Zhao, *J. Mater. Chem. A*, 2018, **6**, 13359–13372.
24 Y. Xu, J. Bao, X. Zhang, W. Li, Y. Xie, S. Sun, W. Zhao and C. Zhao, *J. Colloid Interface Sci.*, 2019, **533**, 526–538.
25 F. E. Ahmed, B. S. Lalia and R. Hashaikeh, *Desalination*, 2015, **356**, 15–30.
26 Y. Yang, X. Yang, L. Liang, Y. Gao, H. Cheng, X. Li, M. Zou, A. Cao, R. Ma, Q. Yuan and X. Duan, *Science*, 2019, **364**, 1057–1062.
27 Z. Tan, S. Chen, X. Peng, L. Zhang and C. Gao, *Science*, 2018, **360**, 518–521.
28 J. Yin, G. Z. Zhu and B. L. Deng, *Desalination*, 2016, **379**, 93–101.
29 H. Kang, W. Wang, J. Shi, Z. W. Xu, H. M. Lv, X. M. Qian, L. Y. Liu, M. L. Jing, F. Y. Li and J. R. Niu, *Appl. Surf. Sci.*, 2019, **465**, 1103–1106.
30 C. S. Guo, N. Li, X. M. Qian, J. Shi, M. L. Jing, K. Y. Teng and Z. W. Xu, *Sep. Purif. Technol.*, 2020, **230**, 115567.
31 J. Wu, Y. J. Zhu, S. W. Cao and F. Chen, *Adv. Mater.*, 2010, **22**, 749–753.
32 J. Wu, Y. J. Zhu and F. Chen, *Small*, 2013, **9**, 2911–2925.
33 B. Q. Lu, Y. J. Zhu, H. Y. Ao, C. Qi and F. Chen, *ACS Appl. Mater. Interfaces*, 2012, **4**, 6968–6973.
34 H. Zhang, Q. Liu, J. Wang, J. Liu, H. Yan, X. Jing and B. Zhang, *RSC Adv.*, 2015, **5**, 5904–5912.
35 E. Kontturi, P. Laaksonen, M. B. Linder, Nonappa, A. H. Groechel, O. J. Rojas and O. Ikkala, *Adv. Mater.*, 2018, **30**, 1703779.
36 A. Tshikovhi, S. B. Mishra and A. K. Mishra, *Int. J. Biol. Macromol.*, 2020, **152**, 616–632.
37 A. W. Carpenter, C. F. de Lannoy and M. R. Wiesner, *Environ. Sci. Technol.*, 2015, **49**, 5277–5287.
38 P. R. Sharma, S. K. Sharma, T. Lindstrom and B. S. Hsiao, *Adv. Sustainable Syst.*, 2020, **4**, 1900114.
39 Z. C. Xiong, Y. J. Zhu, D. D. Qin, F. F. Chen and R. L. Yang, *Small*, 2018, **14**, 1803387.
40 A. Ranjbarzadeh-Dibazar, P. Shokrollahi, J. Barzin and A. Rahimi, *J. Membr. Sci.*, 2014, **470**, 458–469.
41 Q. Q. Zhang, Y. J. Zhu, J. Wu and L. Y. Dong, *ACS Sustainable Chem. Eng.*, 2019, **7**, 17198–17209.
42 P. Zhang, J. L. Gon, G. M. Zeng, B. Song, H. Y. Liu, S. Y. Huan and J. Li, *Chemosphere*, 2018, **204**, 378–389.
43 H. J. Zeng, Z. X. Yua, Y. Peng and L. Zhu, *Appl. Clay Sci.*, 2019, **183**, 105322.
44 S. Y. Fang, P. Zhang, J. L. Gong, L. Tang, G. M. Zeng, B. Song, W. C. Cao, J. Li and J. Ye, *Chem. Eng. J.*, 2020, **385**, 123400.
45 X. Kang, Y. Y. Cheng, Y. Wen, J. Y. Qia and X. Li, *J. Hazard. Mater.*, 2020, **400**, 123121.
46 P. Zhang, J. L. Gong, G. M. Zeng, C. H. Deng, H. C. Yang, H. Y. Liu and S. Y. Huan, *Chem. Eng. J.*, 2017, **322**, 657–666.
47 J. Li, M. Y. Hu, H. C. Pei, X. H. Ma, F. Yan, D. S. Dlamini, Z. Y. Cui, B. Q. He, J. X. Li and H. Matsuyama, *J. Membr. Sci.*, 2020, **595**, 117547.
48 X. J. Yan, W. Tao, S. R. Cheng, C. Ma, Y. Zhang, Y. Sun and X. J. Kong, *Chemosphere*, 2020, **256**, 127118.
49 H. J. Zeng, Z. T. Yu, L. Y. Shao, X. H. Li, M. Zhu, Y. C. Liu, X. F. Feng and X. M. Zhu, *Chem. Eng. J.*, 2021, **403**, 126281.
50 R. N. Zhang, M. R. He, D. H. Gao, Y. N. Liu, M. Y. Wu, Z. W. Jiao, Y. L. Su and Z. Y. Jiang, *J. Membr. Sci.*, 2018, **566**, 258–267.
51 F. Zhong, P. Q. Wang, Y. He, C. L. Chen, H. J. Li, H. Yu and J. Y. Chen, *Polym. Adv. Technol.*, 2019, **30**, 1644–1655.
52 G. J. Zhao, X. M. Wang, C. X. Li and H. Meng, *Appl. Surf. Sci.*, 2020, **508**, 144788.
53 P. K. Samantaray, S. Baloda, G. Madras and S. Bose, *J. Mater. Chem. A*, 2018, **6**, 16664–16679.
54 A. K. Shukla, J. Alam, M. Alhoshan, L. A. Dass, F. A. A. Ali, M. M. R, U. Mishra and M. A. Ansari, *Environ. Sci.: Water Res. Technol.*, 2018, **4**, 438–448.
55 F. Zareei and S. M. Hosseini, *Sep. Purif. Technol.*, 2019, **226**, 48–58.
56 K. Sunil, G. Karunakaran, S. Yadav, M. Padaki, V. Zadorozhnyy and R. K. Pai, *Chem. Eng. J.*, 2018, **348**, 678–684.
57 R. S. Hebbar, A. M. Isloor, K. Anandab and A. F. Ismailc, *J. Mater. Chem. A*, 2016, **4**, 764–774.
58 M. A. Jafar Mazumder, P. H. Raja, A. M. Isloor, M. Usman, S. H. Chowdhury, S. A. Ali and I. A. Al-Ahmed, *Sci. Rep.*, 2020, **10**, 7049.

59 S. Bandehalia, A. Moghadassia, F. Parviziana, Y. T. Zhang, S. M. Hosseinia and J. N. Shen, *Sep. Purif. Technol.*, 2020, **242**, 116745.
60 G. Moradi, S. Zinadini, L. Rajabi and A. A. Derakhshan, *Chem. Eng. J.*, 2020, **390**, 124546.
61 J. E. Efome, D. Rana, T. Matsuura and C. Q. Lan, *J. Mater. Chem. A*, 2018, **6**, 4550–4555.
62 Y. Ibrahim, V. Naddeo, F. Banat and S. W. Hasan, *Sep. Purif. Technol.*, 2020, **250**, 117250.